Russian Journal of Inorganic Chemistry, Vol. 50, No. 1, 2005, pp. 72–77. Translated from Zhurnal Neorganicheskoi Khimii, Vol. 50, No. 1, 2005, pp. 76–81.

PHYSICAL METHODS OF INVESTIGATION

Morphological Selection in Suspensions of Nanocrystalline Hydroxylapatite Leading to Spheroidal Aggregates

A. V. Severin, V. F. Komarov†, V. E. Bozhevol'nov, and I. V. Melikhov

Moscow State University, Vorob'evy gory, Moscow, 119899 Russia

Received January 20, 2004

Abstract—Spontaneous formation of spherical hydroxylapatite (HAP) aggregates with particle diameters from 10 μm to 1–2 mm (mostly, 15–300 μm) is observed in boiling suspensions of nanocrystalline HAP. The material is characterized by electron and atomic-force microscopy and porometry. The particle-size distribution functions for the spherical aggregates are studied as a function of treatment conditions.

Hydroxylapatite (HAP) based materials are applied in medicinal and biochemical practices as sorbents for biopolymers, as biocompatible implants in bone surgery, and as medicine carriers [1, 2]. In some cases, not only the morphology of separate HAP crystals but also the properties of textured forms in which the crystals are aggregated are the key factors in the application efficiency of such materials. Several routes are known to such forms, in particular, to granulated HAP with spherical granules [3–9]. However, binders are required for these routes.

In this study, we consider the aggregation mechanism in aqueous HAP suspensions with the goal of elucidating whether there are routes to govern the texture of the dispersed solid and whether compact aggregates with shapes approaching simple polyhedra or spheres can appear spontaneously. The texture, size, and shape of the aggregates can be changed by mechanically loading the suspension [9–11]. Mechanical loads are most efficient when the forces applied to each aggregate are comparable with the adhesion strength of the suspended particles [12]. The adhesion strength of a particle, which attaches the particle to an aggregate, is affected by the environment in which the particle appears after being attached. When the particle is surrounded by many particles of the aggregate, an increased strength is required to remove it. As a result, loose aggregates are mostly destroyed under mechanical loads in the suspension, while compact aggregates are accumulated: the probability of multiple contacts on the surfaces of compact aggregates is higher than on the loose ones. Mechanostimulated morphological selection of compact aggregates with the simplest shape occurs in this way [13, 14]. One way to achieve thermally enhanced mechanostimulation is to boil the suspension in a bottom-heated, flat-bottomed reactor. In such a reactor, there is a highly overheated zone near the bottom, in which gas bubbles are generated; bubble generation, movement, and collapsing mechanically load the aggregates. The morphological selection probability increases as a result [15, 16]. Boiling induces rather rapid spontaneous formation of spheroidal compact aggregates in aqueous HAP suspensions.

† Deceased.

EXPERIMENTAL

The HAP suspension was prepared using a procedure in [17] by rapidly mixing solutions of the reagents at room temperature under vigorous stirring according to the reaction

$$5Ca(OH)_2 + 3H_3PO_4 = Ca_5(PO_4)_3(OH) + 9H_2O.$$

As a result, platy HAP nanocrystals with average dimensions of $1 \times 70 \times 30$ nm were formed in the system; then, the nanocrystals aggregated [17, 18].

The nanocrystal suspension with 5.5% of the solid phase was exposed for a period from 7 days to 6 months in sealed vessels at 295 K or for 10 days at 370 K without boiling. During this period, the suspension was sampled to be analyzed using optical microscopy (Biolam I, LOMO, Russia), transmission electron microscopy (Jeol JEM-100B, Japan), scanning electron microscopy (Hitachi-S-405, Japan), and atomic-force microscopy (SMENA, NT-MDT, Russia). The results of the investigations were used to determine the particle-size distribution function

$$\varphi(L, t) = \frac{1}{N}\frac{\partial N_L}{\partial L},$$

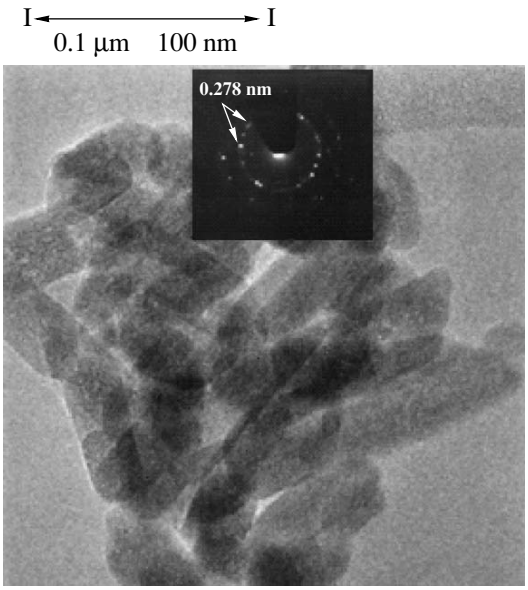

Fig. 1. Aggregates of platy HAP nanoparticles (transmission electron micrograph). $\times(8 \times 10^5)$.

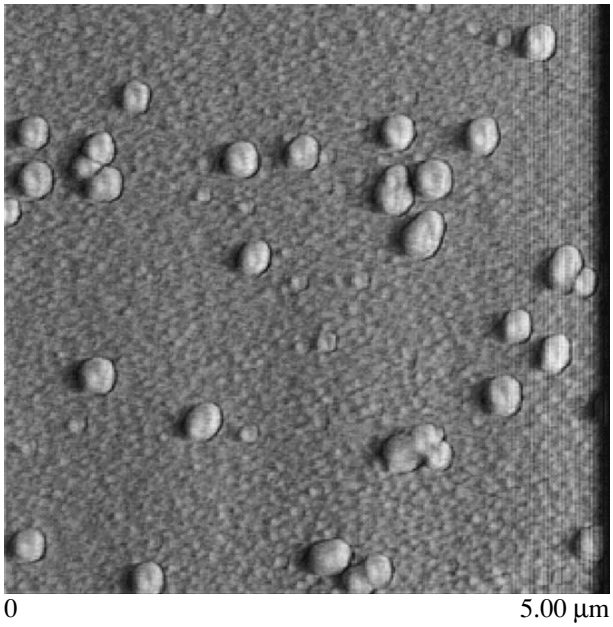

Fig. 2. Compact HAP aggregates (microspheroids) (atomic force micrograph).

the geometric specific surface area of the particles S, and the number of particles in a unit volume of the suspension N_s

$$S = 6\beta\langle L^2\rangle/(\rho\langle L^3\rangle), \quad N_s = 6m_H/(\pi\rho\langle L^3\rangle V_s).$$

Here, N is the number of measured particles; N_L is the number of particles in which the size is less than L, with the size taken equal to the diameter of a circle whose area is equal to the area of the image of the particle viewed with an electron or optical microscope; β is the form-factor; ρ is the HAP weight in a unit volume of the particle; $\langle L^n\rangle = \int_0^\infty L^n \varphi(L, t)dL$ is the moment of the distribution function; m_H is the HAP weight in the suspension; and V_s is the suspension volume.

Portions of the exposed suspension, each 200–300 ml in volume, were transferred into vessels with different shapes and boiled for a period of 1200 to 10 480 s. Spheroidal HAP particles with diameters reaching 2 mm were formed during boiling. After boiling finished, the suspension was allowed to cool to room temperature. The cool suspension was transferred to a coarse filter to suck the mother solution. Then, the spheroidal particles were dried in air at 300 K, with the weight loss being monitored continuously. Air-dry spheroidal particles, which were brought to constant weight (constant-weight particles), were heated at 400 and 1300 K for 3 h, and their weight loss upon heating was determined. The air-dry and heated particles were studied by mercury porometry (on Porosimeter 2000, Germany). The particle-size distribution function for the spheroidal particles was determined microscopically and with a Coulter Multisizer II (France).

RESULTS

Under the conditions studied, HAP crystals in suspension are first aggregated into platy particles (Fig. 1), which are collected in macrofloccules. The floccules sediment, forming a layer with a solid-packing factor of $q = 0.034$. Compact aggregates are formed in the bulk of the floccules (Fig. 2). These aggregates coarsen through attaching platy particles and through coalescing into microparticles of spheroidal shape (microspheroids). At 300 K, almost all the platy particles enter microspheroids in a period of $t \sim 6$ months. The microspheroid size distribution function $\varphi(L, t)$ is shown in

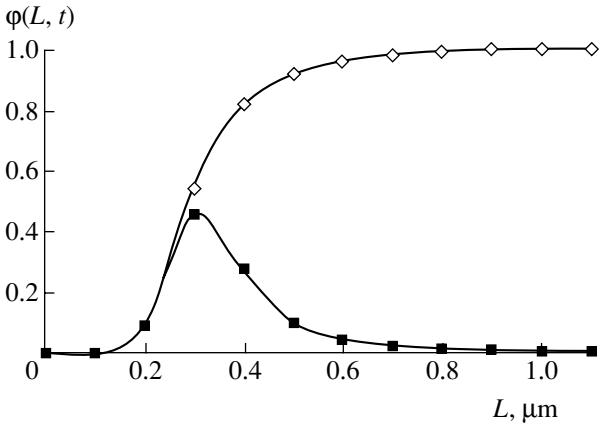

Fig. 3. Microspheroid size distribution function.

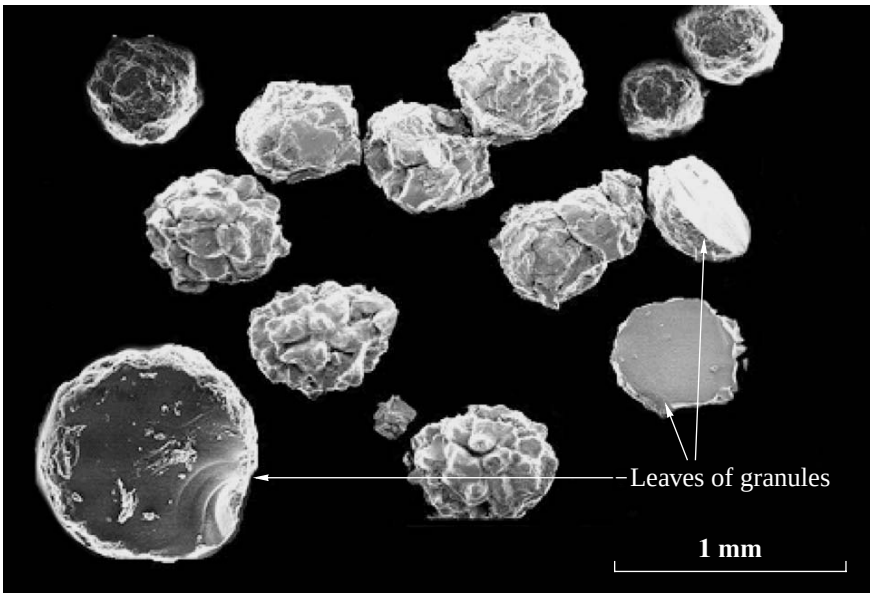

Fig. 4. Macrospheroidal HAP particles (scanning electron microscopy).

Fig. 3. After exposing the suspension without stirring for 7 days at 300 K or for 10 h at 370 K without boiling, particles with sizes $L > 50$ μm are not observed in the suspension. Such particles are formed at a noticeable rate only when the suspension boils in bottom-heated, flat-bottomed vessels. These particles coarsen, acquiring a spheroidal shape and converting to macrospheroids (Fig. 4). The coarsening of the macrospheroids is attended by a decrease in the number of microspheroids (Table 1) and occurs in accordance with

$$\langle L\rangle = L_{\mathrm{M}}\left[1+\left(\frac{L_0}{L_{\mathrm{M}}}-1\right)\exp(-\tau/\tau_0)\right] \qquad (1)$$

for $L_{\mathrm{M}} = AS_s/V_s^{2/3}$.

Here, $\langle L\rangle$ is the average particle size of the suspension; $A = 1400$ μm, $L_0 = 9$ μm, and $\tau_0 = 10800$ s are empirical parameters; S_s is the surface area of the heated bottom; and $\tau = t - t_0$, where t_0 is the moment at which boiling begins.

Table 1. Size L and concentration N_S of HAP aggregates as functions of boiling time τ

τ, min	L, μm	N_S, particles/cm^3
0	1.8 ± 0.2	7.83×10^{10}
20	48 ± 4	1.70×10^{7}
60	120 ± 15	7.40×10^{4}
120	210 ± 20	2.57×10^{4}
180	250 ± 30	1.37×10^{4}

When boiling occurs in a bottom-heated vessel, bubbles are generated at the bottom with the appearance frequency Ω that is proportional to the bottom area:

$$\Omega = W S_s,$$

where W is a variable that characterizes the number of bubbles generated per square meter in a second. From Table 1 and Eq. (1), the aggregate coarsening rate G equals

$$G \equiv \frac{d\langle L\rangle}{dt} = \alpha\frac{(L_{\mathrm{M}}-L_0)}{\tau_0}\left(\frac{N_s-N_{sk}}{N_s}\right), \quad N_s \geq N_{sk}, \qquad (2)$$

where $\alpha = 5.5\times10^3$, and N_s and N_{sk} are the numbers of microspheroids in the suspension at moments $\tau = 0$ and $\tau > 10^4$ s.

The τ_0 value in Eqs. (1) and (2) is the characteristic time of formation for the macrospheroids, platy particles, and microspheroids (Table 2).

In the course of boiling, the $\varphi(L, t)$ function becomes polymodal (Fig. 5). This function is variable and depends crucially on minor changes in the boiling conditions.

The macrospheroids contain significant amounts of water. In particles with sizes 50–300 μm after separating them from the suspension, the water content is 75% of the particle weight. After air drying at 300 K, the water content is reduced irreversibly to 3–5%. The

macrospheroids are contracted when losing water, and their volume is reduced by a value of

$$\Delta V_1 = \frac{\pi}{6} N[\langle L^3 \rangle - \langle L_1^3 \rangle] = (0.83 \pm 0.02)V, \quad (3)$$

where L and L_1 are the particle sizes before and after drying, and $V = (\pi/6)N\langle L^3 \rangle$ is the overall volume of all the macrospheroids measured. When air-dry macrospheroids are heated at 400 K for 3 h, part of the remnant water is removed reversibly. At 1300 K, the water is removed irreversibly and almost completely, and the volume of the macrospheroids is reduced by a value of

$$\Delta V_2 = \frac{\pi}{6} N[\langle L_1^3 \rangle - \langle L_2^3 \rangle] = (0.70 \pm 0.05)V_1, \quad (4)$$

where L_2 is the macrospheroid size after heating, and $V_1 = (\pi/6)N\langle L_1^3 \rangle$.

If the macrospheroids are dried in vacuum at 300 K, all water leaves them in a period longer than 100 h. Such particles have a developed internal pore system with the specific surface area $S_{sp} = 71.0 \pm 3.4$ m^2/g. The specific pore volume inside the macrospheroids, as determined by mercury porometry after evacuating, is 540 ± 60 mm^3/g for an average pore diameter of 38 ± 2 nm.

DISCUSSION

Under the experimental conditions implemented, stagewise morphological selection of compact configurations occurs inside floccules; micro- and macrospheroids are formed as a result of this selection. At an early stage ($\tau_0 \sim 8.6 \times 10^4$ s, 300 K), the amount and size of the microspheroids increase until practically all the platy particles are attached to the microspheroids. The $\varphi(L, t)$ function approaches the curve plotted in Fig. 3. The monomodality of this function indicates that here are almost no platy particles or their small ordered aggregates in the system. At a later stage ($\tau_0 \sim 1200$ s, 370 K), the microspheroids are clustered into macrospheroids. However, the clustering occurs rapidly only when the suspension boils. The formation of macrospheroids from microspheroids is proven by the fact that the number of the microspheroids decreases in association with coarsening of the macrospheroids (Table 1). The kinetics of the microspheroid-to-macrospheroid transition is characterized by Eqs. (1) and (2). The G value may be represented in the form of

$$G = 2\left[\omega \frac{N_s}{N_{s0}} - \nu\right] v_0, \quad (5)$$

where ω is the probability of microspheroid attachment to a macrospheroid in unit time per square meter, ν is the frequency of microspheroid detachment from the macrospheroid (m^{-2} s^{-1}), and v_0 is the volume occupied by the microspheroid inside the macrospheroid.

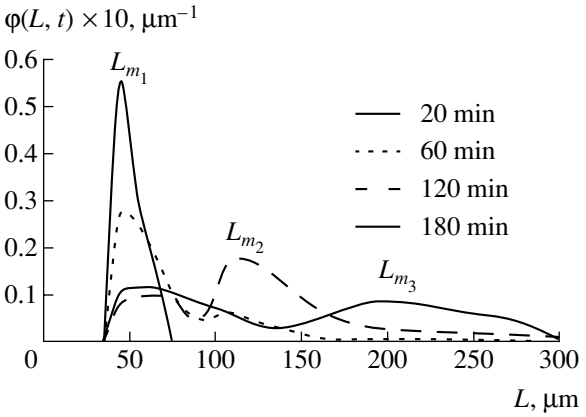

Fig. 5. Evolution of polymodal macrospheroid-size distribution functions with the boiling time.

According to functions (1) and (2), for $\tau \gg \tau_0$, we have $\langle L \rangle \longrightarrow L_m$ and $N_s \longrightarrow N_{sk}$. Therefore,

$$\nu = \omega N_{sk}/N_{s0}, \quad (6)$$

$$\omega = \alpha\left(\frac{A\Omega}{WV_s^{2/3}} - L_0\right)/(2\tau_0 v_0) = 1/(\text{m}^2\ \text{s}). \quad (7)$$

For $N_{sk} \sim N_{s0}$, we have $\omega \sim \nu$; that is, an only insignificant part of the microspheroids that come to the surface of a macrospheroid adhere to the macrospheroid. The other microspheroids leave, which results in morphological selection: only those microspheroids adhere that comply with the requirement of macrospheroid compactness. It seems that the same selection is characteristic of the microspheroids, which also have a compact form (Fig. 2). In the microspheroids, however, morphological selection occurs through thermal motion and natural convective fluxes; in the macrospheroids,

Table 2. Physicochemical characteristics of HAP aggregates of different hierarchic levels

Particle type	T, K	τ_0	Form-factor	Density, g/cm^3	Specific surface area, m^2/g
Nanoplates	298	~10 s	17.9	~3.14	900
Nanoplate aggregates	298	~100 s	2.9	2.03	94
Microspheroids	300	~7 days	1	1.07	89
Macrospheroids	370	20 min	1	1.15	72

through convective fluxes and acoustic fields induced by boiling.

The macrospheroid formation kinetics may be derived from the distribution functions $\varphi(L, t)$ (Fig. 5). At t = 1200–7200 s, this function is bimodal. The first mode ($L_{m1} \sim 50$ μm) retains its position in all experiments; the second mode shifts ($L_{m2} \sim 100$ μm). This means that the aggregates coarsen through pair collisions of microspheroids. Later (t = 10 480 s), the aggregates are involved in pair collisions. The number of macrospheroids with $L_{m2} \sim 100$ μm decreases, and the third mode appears with $L_{m3} \sim 200$ μm. The micro- and macrospheroids are rather compact, which is indicated by the above data and relationship (3).

The macrospheroids have a hierarchic organization. Inside each macrospheroid, constituent microspheroids retain their boundaries; inside each constituent microspheroid, constituent HAP nanocrystals and, probably, some platy particles retain their individuality. This is manifested in the surface relief of the macrospheroids and in the structure of sections and cleaves from macrospheroids (Fig. 4).

When microspheroids stick together, there remain water-filled gaps (macropores) between them. In turn, inside microspheroids there are water inclusions, which can be called micropores. If we take the water density in pores to be the same as the density of free water, we may find the porosity of macrospheroids, associated with the water that occurs in their bulk, from the water weight included in the particles.

$$\varepsilon_A = V_p/V = 1/[1 + m_H\rho_A/(m_A\rho_H)] = 0.91 \pm 0.04. \quad (8)$$

Here, $V = V_P + V_H$; $V_P = m_A/\rho_A$; $V_H = m_H/\rho_H$; and m_A, ρ_A, m_H, and ρ_H are the weight and density of water and HAP, respectively. The water that is removed from macrospheroids upon drying in air at 300 K may be classified with the water in macropores if we set that $V_P = V_{P1} + V_{P2}$, $V_{P1} = (m_A - m_{A1})/\rho_A$, $V_{P2} = m_{A1}/\rho_A$, and

$$\varepsilon_1 = V_{P1}/V = 0.89 \pm 0.04, \varepsilon_2 = V_{P2}/V = 0.02 \pm 0.005, \quad (9)$$

where ε_1 and ε_2 are the contributions of water-filled macro- and micropores to the overall porosity.

It follows from relationships (3) and (9) that the macropores disappear upon drying of the macrospheroids; no pores are seen in cleaves of air-dry macrospheroids (Fig. 4). The disappearance of the pores is also proven by the fact that the macrospheroids are reduced in volume upon drying by a value close to ε_1. Heating eliminates part of the micropores from the macrospheroids, and all of the internal water leaves. Emptied micropores, which do not disappear, govern the porosity of the heated macrospheroids.

$$\varepsilon_F = (V_{P2} - \Delta V_2)/(V - \Delta V_1 - \Delta V_2) = 0.10 \pm 0.02. \quad (10)$$

If water is removed from micropores in vacuum, the internal surface area of the macrospheroids becomes equal to S_{sp} = 71.0 ± 3.4 m^2/g. This surface area approaches the specific surface area of platy aggregates in the suspension at the early aggregation stage (Table 2). This means that, in the bulk of vacuum-dried macrospheroids, boundaries are retained for those platy aggregates that first entered microspheroids and, then, in the composition of these microspheroids, entered macrospheroids. In view of the existence of these boundaries, the micropores in the vacuum-dried macrospheroids may be represented as gaps between platy aggregates. Given that the macrospheroids are low-ordered, the gaps can compare in size with the aggregates; i.e., the gap size can amount to ca. 40 nm, in agreement with mercury porometry data. If we believe that ΔV_1 and ΔV_2 upon vacuum drying have the same values as in air-dry samples and that the gaps do not change their size upon mercury porometry measurements, then the porosity of the vacuum-dry macrospheroids may be set equal to

$$\varepsilon_V = V^v/(V - \Delta V_1 - \Delta V_2) = 0.62 \pm 0.08. \quad (11)$$

Relationships (9)–(11) give an idea of the hierarchic structure of the macrospheroids.

The fact that the macrospheroid volume changes when water is lost indicates that some of the HAP nanocrystals in the bulk of the macrospheroids retain their ability to move relative to each other under the action of relatively small forces. The macrospheroids are bodies having a low tensile strength. The tensile strength is high enough to withstand irreversible changes in the body shapes that are caused by convective fluxes and acoustic fields during boiling, but it is too low for bodies to experience plastic flow under the action of capillary forces during drying. The force of the fluxes applied to each macrospheroid during boiling is only sufficient for the body to flake out the microspheroids and finer macrospheroids that have not found localities with an increased adhesion, but the field has no strength to destroy the aggregate.

To conclude, boiling of suspensions of HAP nanocrystals dramatically enhances the morphological selection, which leads to close-packed macrospheroids with a multilevel internal structure.

REFERENCES

1. H. Li, K. A. Khor, and P. Cheang, Biomaterials **24** (6), 949 (2003).
2. F. Chen, Z. C. Wang, and C. J. Lin, Mater. Lett. **57** (4), 858 (2002).
3. Hsu Fu Yin, Chueh Shan-Chang, and Wang Yng Jiin, Biomaterials **20** (20), 1931 (1999).
4. A. Athanasopoulou, D. Gavril, *et al.*, J. Chromatogr. **A 845** (1–2), 293 (1999).
5. US Patent No. 5,158,756(1992).

6. US Patent No. 5,082,566 (1992).
7. Jpn. Appl. No. 6442311.
8. Hashimoto Kazuaki, Toda Yoshitomo, *et al.* Inorg. Mater. **2** (257), 242 (1995).
9. Patent No. 2 122 520 (1996).
10. E. Rivera-Mnoz, J. R. Diaz, W. Brostow, *et al.*, J. Mater. Sci. **12**, 305 (2001).
11. V. S. Komlev, S. M. Barinov, and E. V. Koplik, Biomaterials **23**, 3449 (2002).
12. B. M. Dolgonosov and I. V. Melikhov, Dokl. Akad. Nauk SSSR **299** (5), 1175 (1988).
13. S. S. Berdonosov, I. A. Kopylova, and I. V. Melikhov, Kolloidn. Zh. **55** (3), 114 (1993).
14. I. V. Melikhov, E. V. Burlakova, and O. V. Kuleshova, Kolloidn. Zh. **53** (2), 375 (1991).
15. M. A. Mikheev, *Fundamentals of Heat Transfer* (Moscow, 1956) [in Russian].
16. S. S. Kutateladze and V. E. Nakoryakov, *Heat and Mass Transfer and Waves in Gas-Liquid Systems* (Novosibirsk, 1984) [in Russian].
17. I. V. Melikhov, V. F. Komarov, V. E. Bozhevol'nov, and A. V. Severin, Dokl. Akad. Nauk **373** (3), 355 (2000).
18. E. I. Suvorova, L. N. Polak, V. F. Komarov, and I. V. Melikhov, Kristallografiya **45** (4), 15 (2000).